Susceptibilities near the QCD (tri)critical point

B.-J. Schaefer[1,2,*] and J. Wambach[2,3]

[1]*Institut für Physik, Karl-Franzens-Universität, A-8010 Graz, Austria*
[2]*Institut für Kernphysik, TU Darmstadt, D-64289 Darmstadt, Germany*
[3]*Gesellschaft für Schwerionenforschung GSI, D-64291 Darmstadt, Germany*

Based on the proper-time renormalization group approach, the scalar and the quark number susceptibilities in the vicinity of possible critical end points of the hadronic phase diagram are investigated in the two-flavor quark-meson model. After discussing the quark-mass dependence of the location of such points, the critical behavior of the in-medium meson masses and quark number density are calculated. The universality classes of the end points are determined by calculating the critical exponents of the susceptibilities. In order to numerically estimate the influence of fluctuations we compare all quantities with results from a mean-field approximation. It is concluded that the region in the phase diagram where the susceptibilities are enhanced is more compressed around the critical end point if fluctuations are included.

I. INTRODUCTION

Theoretical studies reveal an increasing richness in the structure of the phase diagram of strongly interacting matter. At high temperature T and/or quark chemical potential μ it is expected that the system undergoes a phase transition from the ordinary hadronic phase to a chirally restored and deconfined quark gluon plasma (QGP) [1,2]. Other phases such as a two-flavor (2SC) and color-flavor locked (CFL) color-superconducting phase are predicted at high densities and small temperatures. For small chemical potential and high temperature recent lattice calculations suggest the existence of mesonic bound states even above the deconfinement phase transition temperature [3], indicating a strongly coupled QGP.

Based on model calculations [4–7] as well as lattice QCD simulations [8–10], the existence of a critical endpoint (CEP) in the phase diagram is suggested. This is the endpoint of a first-order transition line in the (T, μ)-plane and is a genuine singularity of the QCD free energy. Here the phase transition is of second order, belonging to the three-dimensional Ising universality class. Its precise location, which is e.g. highly sensitive to the value of the strange quark mass, is not known at present. It might be accessible with current and future experimental facilities and its observable implications in relativistic heavy-ion experiments such as event-by-event fluctuations of suitable observables are intensively discussed [11].

From lattice studies it is known that the dynamics of the transition along the temperature axis is strongly affected by the presence of light quarks. The transition temperature is lowered substantially from its value in the pure gauge limit of infinitely heavy quarks, mostly due to the nearly massless up- and down quarks. This indicates a prominent role

of the (nearly exact) chiral $SU(2)_L \times SU(2)_R$ symmetry, which is spontaneously broken to $SU(2)_V$ at small temperatures and baryon densities. Indeed, a chiral phase transition is observed numerically whose transition temperature coincides with that for the deconfinement transition. In the limit of vanishing up- and down quark masses and infinite strange quark mass, the chiral phase transition is likely to be of second-order at vanishing μ and the static critical behavior is expected to fall in the universality class of the Heisenberg $O(4)$ model in three dimensions [12].

Lattice calculation of the QCD phase transition with finite μ is much more difficult. Because of the Fermion sign problem, simulations of similar precision as at $\mu = 0$ are still lacking. From direct numerical evaluation of the QCD partition function and its quantum-statistical analysis [8,9] or from a Taylor expansion of the pressure around $\mu = 0$ there is, however, evidence for a CEP at finite μ. At this point both the chiral- and the quark number susceptibility diverge. The existence of a CEP in the (T, μ)-plane implies that massless two-flavor QCD has a tricritical point (TCP) at which the $O(4)$ line of critical points ends. For larger μ's the transition is then of first-order.

In an attempt to interpret the physical content of the lattice results there is a variety of model studies of the CEP and the critical region around it [13–18]. In future searches for the CEP in heavy-ion reactions the size of the critical region is especially important [19]. Most of these studies rely in one way or another on a mean-field description of the phase transition. As is well known, mean-field theory very often fails to give the correct description of phase transitions and fluctuations have to be included. An efficient way to describe critical phenomena beyond mean-field theory is the renormalization group (RG) method. It can be used to describe the universal and nonuniversal aspects of second-order as well as first-order phase transitions. In the context of the phase diagram of strongly

---

*Electronic address: bernd-jochen.schaefer@uni-graz.at

interacting matter the RG-method has been applied in [20] using a two-flavor quark-meson model, which captures essential chiral aspects of QCD.

Extending our previous analysis, the present work primarily focuses on the question of how large the critical regions around the TCP and CEP might be. The size of a critical region is defined as the one where mean-field theory breaks down and nontrivial critical exponents emerge. A well-known criterion is the Ginzburg criterion which estimates the size by some unknown coupling coefficients. It is based on an expansion of the singular part of the free energy for a second-order phase transition. Since the expansion coefficients, appearing in this criterion are not known for strong interactions the Ginzburg criterion is of limited use in the present context. Also universality arguments are not helpful, if the underlying microscopic dynamics is not well determined. This can be seen, for example, in the λ transition of liquid helium He^4 and the superconducting transition of metals. Both transitions belong to the same universality class of the $O(2)$ spin model but their critical regions defined by their corresponding Ginzburg-Levanyuk temperature τ_{GL}, differ by several orders of magnitude. For hadronic matter it is expected that the critical region of the CEP is small [16]. Here, in this work we will use the enhancement of the chiral and scalar susceptibility as a criterion for the size of the critical region.

The paper is organized as follows. In Sec. III a mean-field analysis of the quark-meson model for two quark flavors as an effective realization of the low-energy sector of QCD is presented. After the derivation of the grand canonical potential for the model, we calculate the phase diagram and localize the CEP. The behavior of the scalar- and pseudoscalar meson masses, the quark number density and the scalar and quark number susceptibilities near the CEP are investigated. In order to obtain a deeper understanding of the shape of the critical region around the CEP, critical exponents are calculated. In Sec. IV we repeat the calculation using the proper-time renormalization group approach (PTRG) in order to assess the influence of fluctuations. Finally, before summarizing in Sec. V, the size of the critical regions around the CEP and TCP are determined and compared with the mean-field results.

II. THE QUARK-MESON MODEL

The Lagrangian of the linear quark-meson model for $N_f = 2$ light quarks $q = (u, d)$ and $N_c = 3$ color degrees of freedom reads

$$\mathcal{L} = \bar{q}(i\slashed{\partial} - g(\sigma + i\gamma_5\vec{\tau}\vec{\pi}))q + \frac{1}{2}(\partial_\mu\sigma\partial^\mu\sigma + \partial_\mu\vec{\pi}\partial^\mu\vec{\pi})$$
$$- U(\sigma, \vec{\pi}) \qquad (1)$$

where the purely mesonic potential is defined as

$$U(\sigma, \vec{\pi}) = \frac{\lambda}{4}(\sigma^2 + \vec{\pi}^2 - v^2)^2 - c\sigma. \qquad (2)$$

The isoscalar-scalar σ field and the three isovector-pseudoscalar pion fields $\vec{\pi}$ together form a chiral 4-component field $\vec{\phi}$. Without the explicit symmetry breaking term c in the potential the Lagrangian is invariant under global chiral $SU(2)_L \times SU(2)_R$ rotations.

The four parameters of the model are chosen such that the chiral symmetry is spontaneously broken in the vacuum and the σ field develops a finite expectation value $\langle\sigma\rangle \equiv f_\pi$, where $f_\pi = 93$ MeV is the pion decay constant. Because of the pseudoscalar character of the pions the corresponding expectation values vanish $\langle\vec{\pi}\rangle = 0$.

The Yukawa coupling constant g is usually fixed by the constituent quark mass in the vacuum $g = M_q/f_\pi$. Using the partially conserved axial vector current (PCAC) relation, the explicit symmetry breaking parameter c is determined by $c = M_\pi^2 f_\pi$, where M_π is the pion mass. The quartic coupling constant λ is given by the sigma mass M_σ via the relation $\lambda = \frac{1}{2f_\pi^2}(M_\sigma^2 - M_\pi^2)$. Finally, the parameter v^2 is found by minimizing the potential in radial direction, yielding $v^2 = \sigma^2 - c/(\lambda\sigma)$. For the ground state where $\langle\sigma\rangle = f_\pi$ this expression can be rewritten as $v^2 = f_\pi^2 - M_\pi^2/\lambda$. It is positive in the Nambu-Goldstone phase.

III. MEAN-FIELD APPROXIMATION

A. The thermodynamic potential

In a spatially uniform system the grand canonical potential (per volume) Ω is a function of the temperature T and of the quark chemical potential μ. We confine ourselves to the $SU(2)_f$-symmetric case and set $\mu \equiv \mu_u = \mu_d$. This is a good approximation since flavor mixing between the u- and d-quark in the vector channel is very small.

The grand canonical potential is obtained as the logarithm of the partition function, which is given by a path-integral over the meson and quark/antiquark fields

$$Z = \int \mathcal{D}\bar{q}\mathcal{D}q\mathcal{D}\sigma\mathcal{D}\vec{\pi} \exp\left\{\int_0^{1/T} dt d^3x(\mathcal{L} + \mu\bar{q}\gamma_0 q)\right\}. \qquad (3)$$

To start with we evaluate the partition function in the mean-field approximation similar to Ref. [21]. Thus we replace the meson fields in Eq. (3) by their expectation values in the action neglecting the quantum and thermal fluctuations of the mesons. The quarks/antiquarks are retained as quantum fields. The integration over the fermions yields a determinant which can be calculated by standard methods (see e.g. Ref. [22]). This generates an effective potential for the mesons. Finally, one obtains

$$\Omega(T, \mu) = -\frac{T\ln Z}{V} = U(\langle\sigma\rangle, \langle\vec{\pi}\rangle) + \Omega_{\bar{q}q}(T, \mu) \qquad (4)$$

with the quark/antiquark contribution

$$\Omega_{\bar{q}q}(T, \mu) = \nu_q T \int \frac{d^3k}{(2\pi)^3} \{\ln(1 - n_q(T, \mu)) + \ln(1 - n_{\bar{q}}(T, \mu))\} \quad (5)$$

where

$$n_q(T, \mu) = \frac{1}{1 + \exp((E_q - \mu)/T)} \quad (6)$$

resp. $n_{\bar{q}}(T, \mu)$ are the usual quark/antiquark occupation numbers with $n_{\bar{q}}(T, \mu) \equiv n_q(T, -\mu)$. The single-particle energy is given by $E_q = \sqrt{\vec{k}^2 + M_q^2}$ and the effective constituent quark mass by $M_q = g\langle\sigma\rangle$. The number of internal quark degrees of freedom is denoted by $\nu_q = 2N_cN_f = 12$.

The divergent vacuum contribution which results from the negative energy states of the Dirac sea has been neglected in Eq. (5). It can be partly absorbed in the mesonic potential up to a logarithmic correction which is largely canceled by a similar logarithmic correction from the quark/antiquark contribution. Accordingly, the omission of the Dirac sea can influence the order of the phase transition for small quark masses (see III B). Since in this work we want to investigate the influence of quantum and thermal fluctuations on top of a completely classical treatment, where all fluctuations and the Dirac sea contribution are neglected, we omit the latter in the mean-field treatment. This omission of the vacuum contribution is in contrast to a similar analysis in the Nambu-Jona-Lasinio model where the vacuum contribution in the corresponding grand canonical potential cannot be neglected due to the finite momentum cutoff regularization [21].

Furthermore, we remark here that the same quark/antiquark contribution of the grand canonical potential can also be obtained by an analytical integration of the corresponding RG flow equation in mean-field approximation [20]. In this simple approximation the mesonic RG flow is neglected and the residual quark/antiquark flow is given by

$$\partial_k \Omega_{\bar{q}q} = -\frac{\nu_q k^4}{12\pi^2} \frac{1}{E_q} \left\{\tanh\left(\frac{E_q - \mu}{2T}\right) + \tanh\left(\frac{E_q + \mu}{2T}\right)\right\}$$
$$= -\frac{\nu_q k^4}{6\pi^2} \frac{1}{E_q} [1 - n_q(T, \mu) - n_{\bar{q}}(T, \mu)], \quad (7)$$

which, after the scale integration towards the infrared, is identical to Eq. (5) if the vacuum contribution is neglected.

For the case of a massless free quark/antiquark gas Eq. (5) can be integrated analytically with the result

$$\lim_{M_q \to 0} \Omega_{\bar{q}q}(T, \mu) = -\frac{\nu_q}{2} \left[\frac{\mu^4}{12\pi^2} + \frac{\mu^2 T^2}{6} + \frac{7\pi^2 T^4}{180}\right]. \quad (8)$$

In general, any phase transition is characterized by an order parameter ϕ which is identified here with the expectation value of the sigma field. Its behavior is determined by the corresponding classical equation of motion. It is obtained by minimizing the potential Ω in radial σ-direction. This results in the gap equation

$$\frac{\partial \Omega}{\partial \sigma} = 0 = \lambda\langle\sigma\rangle(\langle\sigma\rangle^2 - v^2) - c + g\rho_s \quad (9)$$

where the scalar quark density ρ_s has been introduced

$$\rho_s = g\langle\sigma\rangle\nu_q \int \frac{d^3k}{(2\pi)^3} \frac{1}{E_q} \{n_q(T, \mu) + n_{\bar{q}}(T, \mu)\}. \quad (10)$$

[23]

The quark density represents the source term in the equation of motion and can also be calculated analytically for vanishing masses. In this limit, one obtains for the quark density

$$\lim_{M_q \to 0} \frac{\rho_s}{M_q} = \nu_q \left[\frac{T^2}{12} + \frac{\mu^2}{4\pi^2}\right]. \quad (11)$$

B. The phase diagram

The solution of the gap equation (9) determines the behavior of the order parameter as a function of the temperature and the quark chemical potential and thus allows us to study the phase structure of the underlying two-flavor quark-meson model.

In the vacuum we fix the model parameters to $M_\pi = 138$ MeV, $M_\sigma = 600$ MeV, $f_\pi = 93$ MeV, and $M_q = 300$ MeV which result in $c \sim 1.77 \times 10^6$ MeV^3, $v \sim 87.6$ MeV, $\lambda \sim 19.7$, and $g \sim 3.2$.

For a physical pion mass ($M_\pi = 138$ MeV) the model exhibits a smooth crossover on the temperature axis and a first-order chiral phase transition on the density axis. For increasing temperatures this first-order transition line persists up to a critical endpoint (CEP) where the chiral transition becomes second order. Along the line of a first-order phase transition the thermodynamic potential has two minima of equal depth. These minima are separated by a finite potential barrier making the potential nonconvex, which is typical for a mean-field approximation. The height of the barrier is largest at zero temperature and finite quark chemical potential and decreases towards higher temperature. At the critical endpoint the barrier disappears (no latent heat) and the potential flattens. For temperatures above the CEP the transition is washed out and a smooth crossover takes place. With the parameters chosen above the location of the CEP is found to be at $T_c = 91.4$ MeV, $\mu_c = 223$ MeV. In Fig. 1 the phase diagram in the complete (T, μ)-plane is shown.

To study the influence of explicit chiral symmetry breaking we have varied the model parameters keeping the Yukawa coupling g fixed. The resulting phase boundaries are also shown in Fig. 1 for $M_\pi = 100$ MeV and $M_\pi = 69$ MeV (half of the physical pion mass). Reducing the pion mass while keeping the Yukawa coupling fixed, the CEP moves towards the T-axis. This is also the case if the Yukawa coupling is increased and the pion mass is kept
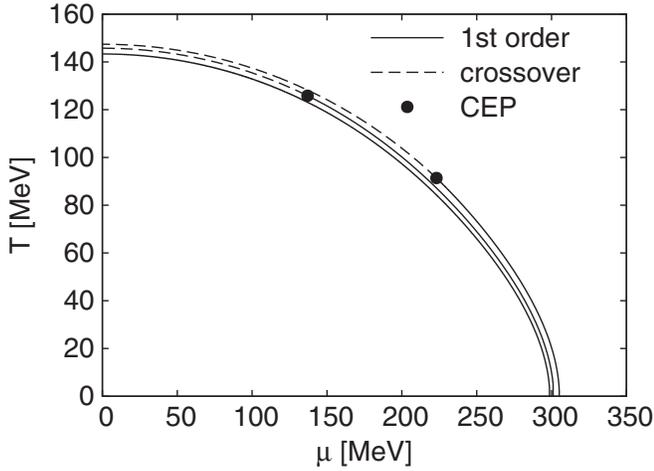
FIG. 1.   The phase diagram of the linear quark-meson model with two constituent quarks in mean-field approximation for three different fits of the pion mass. From top to bottom: $M_\pi = 138, 100, 69$ MeV.

fixed. Already for the pion mass $M_\pi = 69$ MeV the CEP disappears and chiral symmetry is restored via a first-order transition for all temperatures and quark chemical potentials. As a consequence this model does not have a tricritical point in the chiral limit (see also App. C in [24]). This is in contradiction to universality arguments as well as lattice QCD simulations. At vanishing quark chemical potential, the effective theory for the chiral order parameter is the same as for the $O(4)$ model, which has a second-order phase transition [22]. It is further expected that the static critical behavior falls into the universality class of the $O(4)$-symmetric Heisenberg model in three dimensions [12].

But, as already stated in Ref. [21], within the mean-field approximation the order of the phase transition in the chiral limit of the linear quark-meson model strongly depends on the values for the model parameters. The way how to extrapolate towards the chiral limit is not unique. As we shall see below, the mean-field approximation itself is also questionable.

C. In-medium meson masses

To gain further physical insight into the critical behavior of the model we have studied the ''in-medium'' meson masses $M_\pi(T, \mu)$ and $M_\sigma(T, \mu)$, which encode the critical fluctuations of the matter. The in-medium meson masses are defined by the second derivative of the grand canonical potential w.r.t the corresponding fields at the global minimum:

$$M^2_{\pi_i}(T, \mu) = \left.\frac{\partial^2 \Omega(T, \mu)}{\partial \pi_i \partial \pi_i}\right|_{min},$$

$$M^2_\sigma(T, \mu) = \left.\frac{\partial^2 \Omega(T, \mu)}{\partial \sigma \partial \sigma}\right|_{min}.$$

In Fig. 2 the temperature dependence of the meson masses for three different chemical potentials are shown. The sigma mass always decreases with temperature in the hadronic (chirally broken) phase and increases again at high temperature. The pion mass does not vary much below the transition but increases at high temperatures similar to the sigma mass indicating the restoration of chiral symmetry. The increase of the sigma and pion mass at high temperature is driven by the asymptotic behavior of the scalar quark density [see Eq. (11)] because chiral symmetry restoration enforces a decrease of the constituent quark mass. At large temperature the meson masses degenerate and increase linearly with T. A similar behavior is seen for the corresponding screening masses on the lattice at $\mu = 0$ [25].

Figure 3 shows the chemical potential dependence of the meson masses for three different temperatures analogous to Fig. 2. For small temperatures a discontinuity is visible in the evolution of the masses, signaling a first-order phase transition. At $T = 0$ and small μ the masses are constant and equal to the vacuum masses which can also be seen analytically. At the CEP the phase transition is of second order. Second-order phase transitions are characterized by long-wavelength fluctuations of the order parameter. Since the order parameter is proportional to the scalar σ-field, the corresponding scalar sigma mass must vanish at this point. In the vicinity of this point the sigma mass drops below the pion mass and the potential flattens in the radial direction. This behavior can clearly be seen in both Figs. 2 and 3. Since chiral symmetry is still explicitly broken the pseudoscalar mass stays always finite. For temperatures above the chiral transition the sigma mass drops below the pion mass and increases with the chemical potential (cf. Figs. 2 and 3). Close to μ_c for $\mu = 300$ MeV in
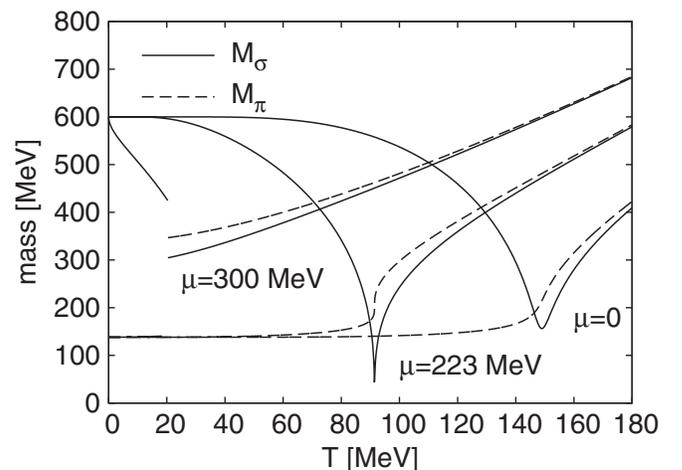
FIG. 2.   The pion and sigma masses as function of the temperature for three different quark chemical potentials ($\mu = 0$, $\mu = \mu_c \sim 223$, and $\mu = 300$ MeV). In the vicinity of the CEP (at μ_c and $T_c \sim 91$ MeV) the sigma mass M_σ vanishes.
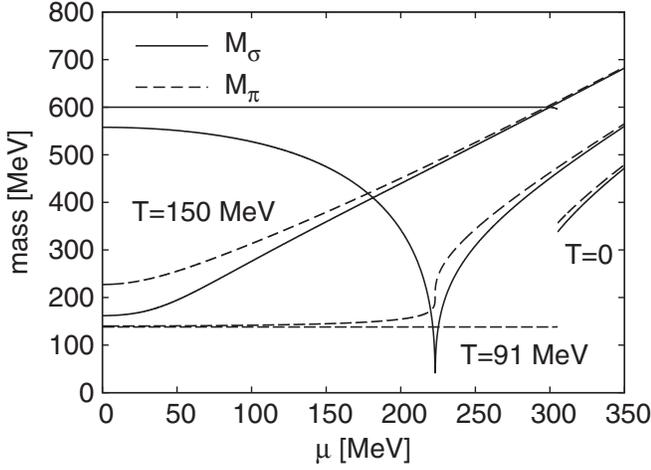
FIG. 3. Similar to Fig. 2: The pion and sigma masses as functions of the chemical potential for three different temperatures ($T = 0$, $T = T_c \sim 91$, and $T = 150$ MeV).

Fig. 2 the sigma mass drops rapidly with temperature and jumps at the chiral transition.

D. Susceptibilities

In order to find a bound to the size of the critical region around the CEP we calculate the quark number susceptibility χ_q and its critical behavior. In general, the quark number susceptibility is the response of the quark number density $n(T, \mu)$ to an infinitesimal variation of the quark chemical potential

$$\chi_q(T, \mu) = \frac{\partial n(T, \mu)}{\partial \mu}. \quad (12)$$

Before we study the thermodynamic properties of the susceptibility, we start with an analysis of the (total) quark number density $n(T, \mu)$. It is defined by a derivative w.r.t. the quark chemical potential of the grand canonical potential (4)

$$n(T, \mu) = \langle q^\dagger q \rangle = -\frac{\partial \Omega(T, \mu)}{\partial \mu}$$

$$= \nu_q \int \frac{d^3k}{(2\pi)^3} \{n_q(T, \mu) - n_{\bar{q}}(T, \mu)\}. \quad (13)$$

For $T \to 0$ and $\mu \to 0$ respectively, the analytical results for the quark number density are

$$n(0, \mu) = \frac{\nu_q}{6\pi^2}(\mu^2 - M_q^2)^{3/2}\theta(\mu - M_q), \quad (14)$$

$$n(T, 0) = 0. \quad (15)$$

For a massless free quark gas one obtains for the density

$$\lim_{M_q \to 0} n(T, \mu) = \frac{\nu_q}{6}\mu\left[T^2 + \frac{\mu^2}{\pi^2}\right]. \quad (16)$$

In Fig. 4 the quark number density in mean-field approximation is shown for three different temperatures around the CEP. For $T = T_c$ the slope tends to infinity at $\mu = \mu_c$ which will yield a diverging susceptibility. For temperatures below the critical one the system undergoes a first-order phase transition and the quark number density jumps. The slope of the quark density in the chirally symmetric phase is almost constant for all temperatures around the CEP. For temperatures above the CEP the discontinuity vanishes at the transition and the density changes gradually due to the smooth crossover. This produces a finite height of the quark number susceptibility χ_q which is calculated via Eq. (12). The resulting susceptibilities are shown in Fig. 5.

For $\mu = 0$ the susceptibility $\chi_q(T, 0)$ increases as the quark mass $M_q(T)$ decreases and reaches $N_f T^2$ at $M_q(T) = 0$ for three colors. χ_q diverges only at the CEP and is finite everywhere else. The height of χ_q decreases for decreasing chemical potentials above the CEP towards the T-axis. For temperatures below the CEP χ_q is discontinuous and jumps across the first-order transition line.

It is instructive to note that the quark number susceptibility is proportional to the isothermal compressibility κ_T via the relation

$$\kappa_T = \chi_q(T, \mu)/n^2(T, \mu). \quad (17)$$

In the vicinity of the critical point the quark number density n is always finite but the susceptibility becomes large. This indicates that the system is easy to compress around the critical point [26].

It is also possible to express the quark number susceptibility as an integral over the quark/antiquark occupation numbers (6)
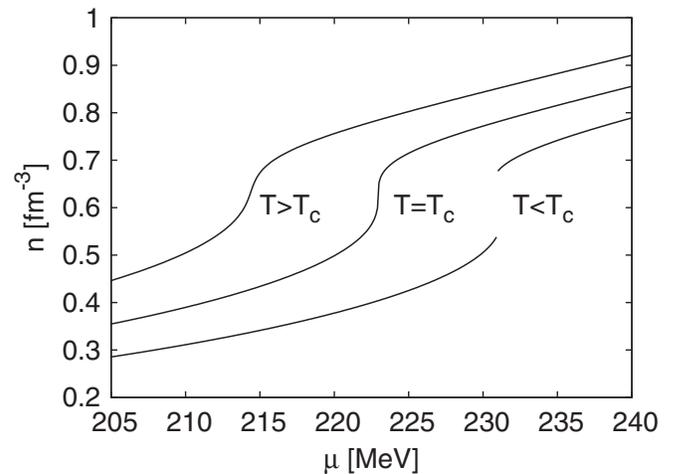
FIG. 4. The quark number density n in mean-field theory as a function of the chemical potential μ around the CEP for three different temperatures. The temperatures are $T_c \sim 91$ MeV and $T = T_c \pm 5$ MeV.
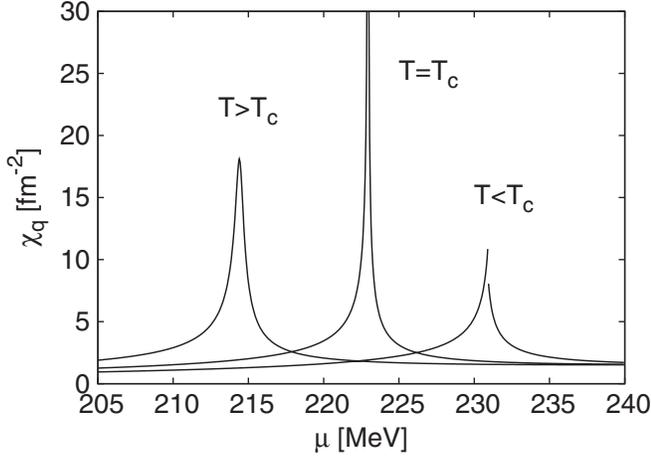
FIG. 5. The quark number susceptibility in mean-field approximation as a function of the chemical potential around the CEP for three temperatures. The temperatures are the same as in Fig. 4. (See text for details).

FIG. 6. The contour regions for two different ratios of the quark number susceptibilities $R_q = \chi_q(T, \mu)/\chi_q^{\text{free}}(T, \mu)$ ($R_q = 3$ and 5) in mean-field approximation around the CEP.

$$\chi_q(T, \mu) = \frac{\nu_q}{T} \int \frac{d^3k}{(2\pi)^3} \{n_q(T, \mu)(1 - n_q(T, \mu))$$
$$+ n_{\bar{q}}(T, \mu)(1 - n_{\bar{q}}(T, \mu))\} \qquad (18)$$

with the corresponding limits

$$\chi_q(0, \mu) = \frac{\nu_q}{2\pi^2} \mu \sqrt{\mu^2 - M_q^2} \theta(\mu - M_q), \qquad (19)$$

$$\chi_q(T, 0) = \frac{\nu_q}{T} \int \frac{d^3k}{(2\pi)^3} \frac{1}{1 + \cosh(E_q/T)}, \qquad (20)$$

$$\lim_{M_q \to 0} \chi_q(T, \mu) = \frac{\nu_q}{6} \left[T^2 + \frac{3\mu^2}{\pi^2} \right] \equiv \chi_q^{\text{free}}. \qquad (21)$$

For an estimate of the critical region around the CEP we have calculated the dimensionless ratio of the susceptibility and its massless free quark gas limit [cf. Eq. (21)]

$$R_q(T, \mu) = \frac{\chi_q(T, \mu)}{\chi_q^{\text{free}}(T, \mu)}. \qquad (22)$$

Figure 6 shows a contour plot for two fixed ratios R_q in the phase diagram near the CEP. A constituent quark mass of roughly 300 MeV has been chosen. The region of enhanced χ_q is elongated in the direction parallel to the first-order transition line.

In order to compare this behavior of the quark number susceptibility around the CEP we repeat the previous analysis with the scalar susceptibility. In general, static susceptibilities are obtained of the dynamic response function $\chi_{ab}(\omega, \vec{q})$ in the static and long wavelength limit

$$\chi_{ab} = -\frac{1}{V} \frac{\partial^2 \Omega}{\partial a \partial b} = \lim_{\vec{q} \to 0} \chi_{ab}(0, \vec{q}), \qquad (23)$$

where a, b denote external fields [24]. The scalar susceptibility χ_σ corresponds to the zero-momentum projection of the scalar propagator, which encodes all fluctuations of the order parameter. The scalar susceptibility is related to the order parameter by

$$\chi_\sigma = \frac{\partial \langle \bar{q}q \rangle}{\partial m_q} = -\frac{\partial^2 \Omega}{\partial m_q^2}. \qquad (24)$$

As a function of temperature or quark chemical potential the maximum of χ_σ should coincide with the most rapid change in the chiral order parameter. One easily verifies that the scalar susceptibility is related to the sigma mass via $\chi_\sigma \sim M_\sigma^{-2}$.

Similar equations can also be formulated for the pseudoscalar susceptibility χ_π, which is related to the order parameter via a Ward identity

$$\chi_\pi = \langle \bar{q}q \rangle / m_q. \qquad (25)$$

In the chiral limit the divergence of the pseudoscalar (transverse) susceptibility χ_π in the broken phase signals the appearance of massless (Goldstone) modes.

In Fig. 7 the contour region of the normalized scalar susceptibility

$$R_s(T, \mu) = \frac{\chi_\sigma(T, \mu)}{\chi_\sigma(0, 0)} \qquad (26)$$

is shown for four fixed ratios around the CEP. Again we observe an elongated critical region in the phase diagram, where χ_σ is enhanced in the direction parallel to the first-order transition line. The deeper reason for this feature can be understood by a study of the critical exponent of the susceptibility at the critical point which will be done in the next section.
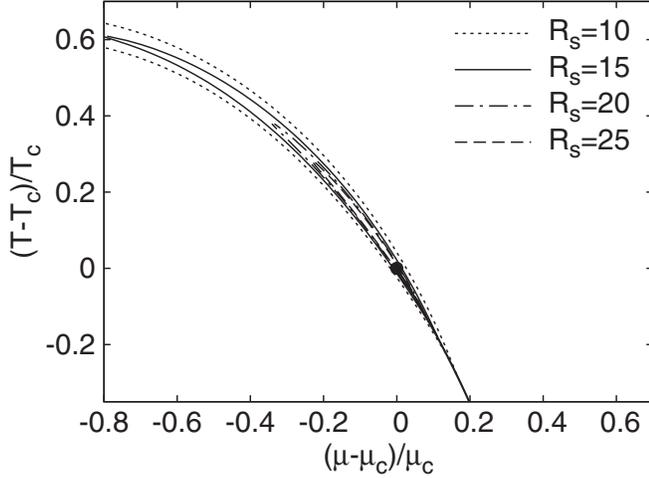
FIG. 7. Same as Fig. 6 for four different ratios of the scalar susceptibilities $R_s = \chi_\sigma(T, \mu)/\chi_\sigma(0,0)$ ($R_s = 10, 15, 20, 25$).

FIG. 8. The logarithm of the quark number susceptibility χ_q as a function of $\ln|\mu - \mu_c|$ at the CEP in mean-field approximation. The solid line is a linear fit.

E. Critical exponents

Since the quark-meson model in mean-field approximation does not exhibit a tricritical point in the chiral limit we focus on the critical behavior of the susceptibility in the vicinity of the CEP. At that point the quark number susceptibility diverges with a certain critical exponent. But a crucial observation is the following: In general, the form of this divergence depends on the route by which one approaches the critical point [27]. For the path asymptotically parallel to the first-order transition line the divergence of the quark number susceptibility scales with an exponent γ_q. In mean-field approximation one expects $\gamma_q = 1$ for this path. For any other path, not parallel to the first-order line, the divergence scales with the exponent $\epsilon = 1 - 1/\delta$. Thus, in mean-field approximation $\epsilon = 2/3$ because $\delta = 3$ and therefore $\gamma_q > \epsilon$. This is the reason for the elongated shape of the critical region in the phase diagram (cf. Figs. 6 and 7) and why χ_q is enhanced in the direction parallel to the first-order transition line.

In order to confirm this behavior we have calculated the critical exponent of the quark number susceptibility χ_q numerically. We have used a path parallel to the μ-axis in the (T, μ)-plane from lower μ towards the critical $\mu_c \sim 223$ MeV at fixed temperature $T_c \sim 91.4$ MeV. Figure 8 shows the logarithm of χ_q as a function of μ close to the CEP for a fixed constituent quark mass. Using a linear logarithmic fit we obtain

$$\ln \chi_q = -\epsilon \ln|\mu - \mu_c| + r, \qquad (27)$$

where the term r is independent of μ. We observe scaling over several orders of magnitude (only two orders are shown in the Figure) and obtain $\epsilon = 0.64 \pm 0.02$, which is in good agreement with the mean-field prediction $\epsilon = 2/3$. The scaling close to the critical point is also demonstrated in Fig. 8. The onset of scaling is around $\ln|\mu - \mu_c| < -1$ which is not shown in the figure.
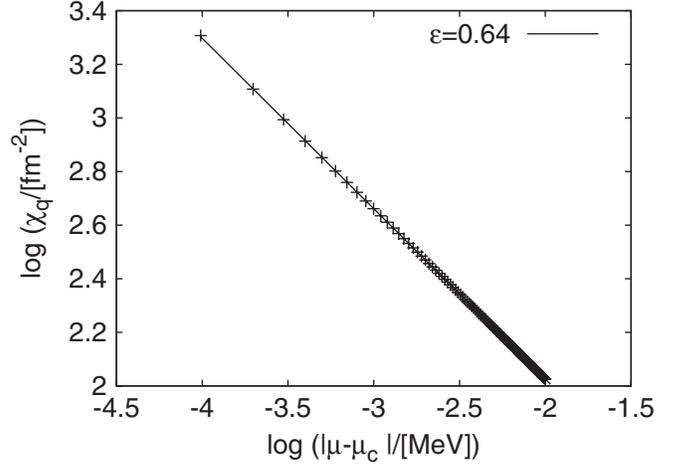
IV. PROPER-TIME RG APPROACH

In this section we study the phase diagram of the quark-meson model within the PTRG approach in the chiral limit as well as for realistic pion masses. In order to study the influence of fluctuations we will repeat the calculations of all previous quantities near the critical endpoint in the phase diagram.

As we have seen, the mean-field approximation fails to properly describe the expected critical physics in the chiral limit (at least for the parameter set chosen). We will show, that this is remedied in the RG approach and a second-order transition in the chiral limit at finite temperature and zero chemical potential is found. This transition lies in the $O(4)$ universality class, as expected. For nonzero chemical potential the second-order transition ends in a TCP and becomes a smooth crossover for finite quark (pion) masses with a CEP. Thus, by variation of the pion mass the relationship and the correlations between the TCP and the CEP's can be studied. In addition, the influence of fluctuations on the susceptibilities and the critical region around the CEP can be assessed.

In order to include fluctuations we use the proper-time renormalization group (PTRG) method [28–33]. In the vacuum, the PTRG flow equation for the scale-dependent effective action $\Gamma_k[\Phi]$ is governed by the self-consistent equation

$$\partial_t \Gamma_k[\Phi] = -\frac{1}{2} \int_0^\infty \frac{d\tau}{\tau}[\partial_t f_k(\tau k^2)] \operatorname{tr} \exp(-\tau \Gamma_k^{(2)}[\Phi]),$$

where $\Gamma_k^{(2)}$ represents the full inverse propagator and is given by a second functional derivative w.r.t. the field components Φ. The smearing function is labeled by $f_k(\tau k^2)$ and tr denotes a four-dimensional momentum integration and a trace over all given inner spaces (e.g. Dirac, color and/or flavor-space). Details and the generalization to

finite temperature and chemical potential can be found e.g. in Refs. [20,29].

For the quark-meson model (1) the resulting flow equation for the scale-dependent grand canonical potential $\Omega_k(T, \mu)$ is given by

$$\partial_t \Omega_k(T, \mu) = \frac{k^5}{12\pi^2} \left[\frac{3}{E_\pi} \coth\left(\frac{E_\pi}{2T}\right) + \frac{1}{E_\sigma} \coth\left(\frac{E_\sigma}{2T}\right) \right.$$
$$- \frac{2N_c N_f}{E_q} \left\{ \tanh\left(\frac{E_q - \mu}{2T}\right) \right.$$
$$\left. \left. + \tanh\left(\frac{E_q + \mu}{2T}\right) \right\} \right], \qquad (28)$$

with the pion-$E_\pi = \sqrt{k^2 + 2\Omega_k'}$, the σ-meson $E_\sigma = \sqrt{k^2 + 2\Omega_k' + 4\phi^2 \Omega_k''}$ and quark energies $E_q = \sqrt{k^2 + g^2 \phi^2}$. The primed potential denotes the ϕ^2-derivative of the potential, i.e., $\Omega_k' := \partial \Omega_k / \partial \phi^2$ and correspondingly the higher derivatives.

We solve the flow equation (28) by discretizing the generally unknown potential Ω_k on a ϕ^2-grid. For details concerning the numerical implementations we refer the interested reader to Refs. [20,34] and references therein.

For the results presented below we have chosen an UV cutoff $\Lambda = 500$ MeV and have fixed the quartic coupling to $\lambda = 11.5$ in order to reproduce a pion decay constant $f_\pi \sim 87$ MeV in the chiral limit. The running of the Yukawa coupling g is neglected here and fixed to $g = 4.2$ in order to reproduce a constituent quark mass of the order of 370 MeV. Note, that this value of the quark mass is roughly 100 MeV larger than the one used in the previous work [20]. As a consequence, the tricritical point in the phase diagram moves to larger temperatures and smaller chemical potentials.

A. The phase diagram

In the present work we have also generalized previous results in the chiral limit [20] to finite pion masses. The resulting phase diagrams for the chiral limit and for physical pion masses $M_\pi \sim 130$ MeV are both shown in Fig. 9. In the chiral limit a second-order phase transition (dashed line) belonging to the $O(4)$-universality class is found. For zero chemical potential we find a critical temperature $T_c \sim 170$ MeV for two massless quark flavors, in good agreement with lattice simulations [35]. For increasing chemical potential the second-order transition line ends in a TCP (bullet).

For our choice of parameters the location of the TCP is at $T_c^t \sim 80$ MeV and $\mu_c^t = 268$ MeV. For temperatures below the TCP the phase transition changes initially to a first-order transition (solid line). For temperatures below $T_s \sim 10$ MeV two phase transitions with a further tricritical point (labeled as "2nd TCP" in the figure) emerge as already described in Ref. [20]. A larger constituent quark
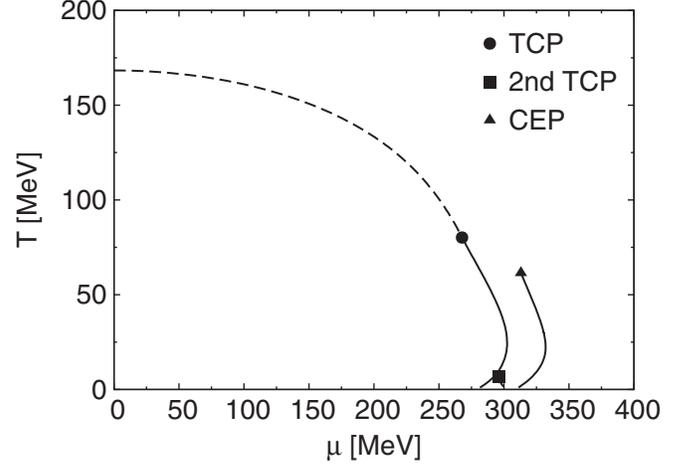
FIG. 9. Two phase diagrams of the linear $N_f = 2$ quark-meson model: One for physical pion masses (right solid line which ends in the CEP) and another one for the chiral limit. Solid lines denote first-order and dashed lines second-order transition lines (see text for details).

mass pushes the location of the TCP towards the temperature axis and the location of the splitting point down towards the chemical potential axis. All qualitative properties of the two phase transitions below the splitting point survive. Only the area bounded by the transition lines is reduced for increasing quark masses (cf. phase diagram in Ref. [20]).

As the pions become massive the TCP turns into a CEP. For each value of the pion mass there is a corresponding CEP. In an extended, three-dimensional (T, μ, m_π) phase diagram these points arrange into a critical line (the "wing critical line"). It is expected that the static critical behavior of this line falls into the universality class of the Ising model in three dimensions corresponding to the one-component ϕ^4-theory in 3D. For the coupling constants listed above we obtain $M_\pi \sim 123$ MeV, $M_\sigma \sim 520$ MeV, and $M_q \sim 390$ MeV in the vacuum and the location of the CEP is at $T_c^c \sim 61.5$ MeV and $\mu_c^c \sim 313.1$ MeV. A better fit to the physical pion mass can be accomplished by a fine tuning of the initial coupling constants. Later a comparison with the results of the previous mean-field analysis is made. We therefore tried to fix the coupling constants in such a way to obtain almost the same vacuum meson masses, constituent quark mass and pion decay constant as in the mean-field approximation. Although there are slight deviations in these numbers all qualitative statements will stay valid.

Compared to recent lattice and other model studies (cf. Fig. 6 in Ref. [2]) the location of the TCP and consequently of the CEP is at lower temperatures due to omission of other degrees of freedom in the quark-meson model.

For any finite value of the symmetry breaking parameter c in the potential (2) the critical $O(4)$-line is immediately

washed out and turns into a smooth crossover line which is not visible in the phase diagram. For temperatures below the CEP a first-order curved transition line is found which persists down to the μ-axis. In the chiral limit below the splitting point, the right second-order transition turns into a crossover for finite quark masses and is again not visible in the phase diagram anymore. Analogously, the second tricritical point, if it exists, should turn into a critical point. Some remnants of this critical point can indeed be seen in the vacuum expectation value and meson masses. But a detailed analysis of this point is postponed to a future work. In the following we focus of the region around the TCP and CEP.

B. In-medium meson masses

The scale-dependent in-medium sigma and pion masses are determined by the curvature of the potential Ω at the global minimum ϕ_0 via the relations

$$M^2_{\pi,k} = 2\Omega'_k|_{\phi=\phi_0}, \qquad M^2_{\sigma,k} = (2\Omega'_k + 4\phi^2\Omega''_k)|_{\phi=\phi_0}. \tag{29}$$

In Fig. 10 the meson masses are shown as a function of temperature for two different chemical potentials similar to Fig. 2. For $\mu = 0$ the sigma mass drops relatively quickly with temperature while the pion mass are almost constant in the chirally broken phase. This behavior is very similar to a PTRG analysis with another smearing function and a truncation of the meson potential (cf. Fig. 14 in [29]). For $\mu = \mu_c^c \sim 313$ MeV and at $T = 0$ the sigma mass is almost degenerate with the pion mass $M_\pi \sim 150$ MeV (see Fig. 10). For increasing temperatures, the sigma mass jumps to almost its vacuum value as it crosses the first-order phase transition. In the vicinity of the CEP around $T \sim 60$ MeV the sigma mass drops below the pion mass
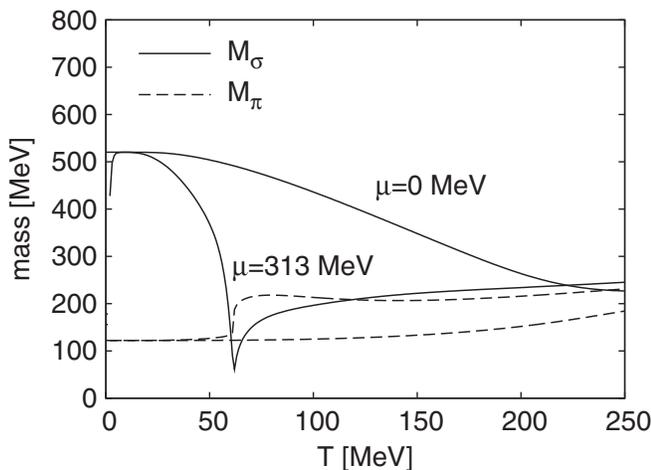
and vanishes at the critical point. At this point the potential in the radial direction around the global minimum becomes flat. As in the mean-field approximation the slope of the sigma mass as function of temperature (or of the chemical potential) at the CEP tends to infinity.

In Fig. 11 the meson masses parallel to the μ-axis for three different temperature slices ($T = 1$, $T = T_c^c$, and $T = 150$ MeV) in the phase diagram are shown. For $T = 1$ MeV the sigma mass is constant and slightly before the first-order transition a melting of the mass takes place.

Because of the curved first-order transition line the critical chemical potential at the CEP around $T \sim 61$ MeV coincides with the critical chemical potential at $T = 1$ MeV.

One important observation is that the sigma mass drops to zero around the CEP much faster if fluctuations are included.

C. Susceptibilities

In the vicinity of critical phenomena, fluctuations that are neglected in a mean-field approximation become more and more important. In order to study the modifications, induced by the fluctuations, we have recalculated the quark number density and susceptibilities within the RG method. It should be recapitulated that, in contrast to the mean-field approximation, this method yields a TCP in the phase diagram for the chiral limit.

In the following we begin our investigations with the chiral limit. In Fig. 12 the density n is shown as function of μ for three different temperatures around the TCP.

For temperatures below the tricritical T_c^t n jumps due to the first-order transition. Above the tricritical temperature there is a kink in the density due to the second-order nature of the transition. In the symmetric phase n grows almost linearly. At the TCP the slope of the density when ap-

FIG. 10. The pion and sigma masses as a function of temperature for two different quark chemical potentials ($\mu = 0$ and $\mu = \mu_c^c \sim 313$ MeV). Near the CEP (located at μ_c^c and $T_c^c \sim 61.5$ MeV) M_σ vanishes.
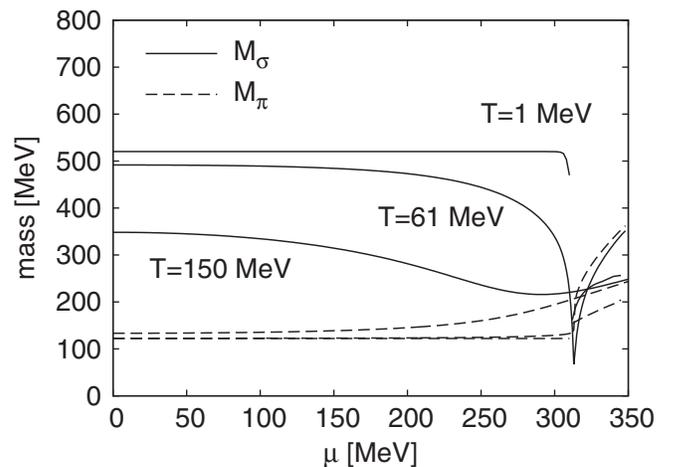
FIG. 11. Similar to Fig. 10: The pion and sigma masses as a function of chemical potential for three different temperatures ($T = 1$, $T = T_c^c \sim 61$, and $T = 150$ MeV).
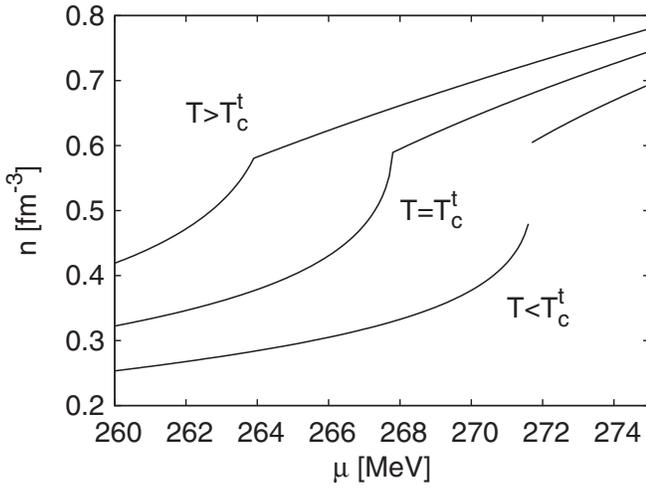
FIG. 12. The quark number density around the TCP. The three temperatures are $T_c^t = 80.2$ MeV and $T = T_c^t \pm 5$ MeV.

FIG. 14. The quark number density around the CEP. The three temperatures are $T_c^c = 61.5$ MeV and $T = T_c^c \pm 5$ MeV.

proached from the broken phase, diverges thus yielding a divergent susceptibility. This is demonstrated in Fig. 13 where the chemical potential dependence of the quark number susceptibility is shown for three different fixed temperatures around the TCP.

In the chiral limit, the susceptibility always jumps across the first- or the second-order transition. In Fig. 13 the second-order transition jump of χ_q is drawn with solid lines. Far below the chiral phase transition χ_q is suppressed. In the restored phase χ_q tends towards the value of the massless free quark gas, χ_q^{free}, Eq. (21).

When we now leave the chiral limit and investigate the phase diagram around the CEP, the critical behavior of the transition changes. In contrast to the behavior of the quark number density around the TCP it does not have any kink at finite quark masses (cf. Fig. 14).

For temperatures below the critical T_c^c, the density jumps again at the phase transition due to its first-order character. But above the CEP the discontinuity vanishes at the transition and the system runs through a smooth crossover. For temperatures above T_c^c, the slope of the density is always finite, except exactly at T_c^c where it diverges yielding a divergent quark number susceptibility at this point. Thus, the divergence of χ_q survives even at finite quark masses. The finite slope results in a finite peak of χ_q which is shown in Fig. 15 where the quark number susceptibility for three different temperatures around the CEP, similar to Fig. 13, is displayed.

Below the chiral transition, the susceptibility is again suppressed and in the restored phase it tends towards χ_q^{free} of a massless free quark gas. Only at the first-order transition there is a discontinuity. In contrast to the chiral limit,

FIG. 13. The quark number susceptibility around the TCP. The three temperatures are the same as in Fig. 12.
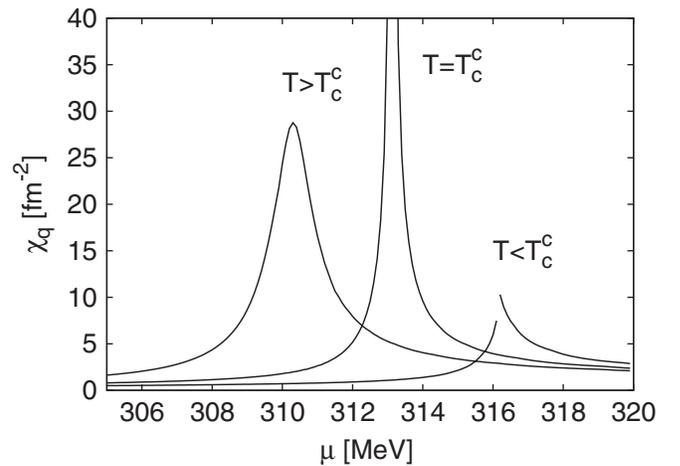
FIG. 15. The quark number susceptibility around the CEP as a function of chemical potential for three fixed temperatures. The three temperatures are $T_c^c = 61.5$ MeV and $T = T_c^c \pm 5$ MeV.

the quark susceptibility is a smooth continuous function for temperatures above the CEP.

On the lattice a similar behavior of the quark susceptibility is seen [36,37]. At $\mu = 0$, χ_q increases smoothly near the critical temperature. At finite chemical potential it develops a pronounced dip but with increased error bars around the transition temperature. On the other side, a significant peak in the isovector channel is not seen on the lattice. Thus, this indicates that only one scalar degree of freedom becomes massless at this point. Also universality arguments predict that the susceptibility diverges at both the TCP and CEP with certain but different critical exponents. At the TCP χ_q should show a power-law behavior with a critical exponent γ_q. Since the TCP belongs to a Gaussian fixed point mean-field exponents are expected.

In the chiral limit the susceptibility χ_q always has a discontinuous jump across the critical $O(4)$-transition line. χ_q is larger below the $O(4)$-line (in the chirally broken phase) than in the restored phase. At any finite μ the susceptibility has a cusp at the critical $O(4)$-transition line. The peak of this cusp on the critical line as approached from the broken phase becomes higher and higher as we increase μ. Finally, it diverges exactly at the TCP, while the potential and thus the pressure will stay finite. Only at $\mu = 0$, the quark number susceptibility is a continuous function across the phase boundary.

On the other side, as already mentioned, in the chirally symmetric phase, χ_q tends towards the value of the massless free quark-gas susceptibility χ_q^{free}. The deviations are caused by the residual meson interaction in this phase.

D. Critical exponents

For finite quark masses it is expected that the universality class of the critical points changes. In order to determine the universality class of the TCP and CEP we have also calculated the corresponding critical exponents of the quark number susceptibility. In determining the critical exponent we proceed in exactly the same way as described in the mean-field section. The calculation of the first and second derivative of the potential for the quark number density and susceptibility is again determined numerically with an adaptive step size algorithm in order to minimize rounding and truncation errors.

We again begin the analysis with the chiral limit. We have used a path parallel to the μ-axis in the (T, μ)-plane from lower μ towards the TCP. Note, that in the (T, μ)-plane the first-order transition line and the critical $O(4)$-line at the TCP are asymptotically parallel and are not parallel to either the T- or μ-axis.

Using a linear logarithmic fit of χ_q in the vicinity of the TCP we obtain the critical exponent $\gamma_q = 0.53$ which is shown in Fig. 16. The region where the scaling starts is rather small $|\mu - \mu_c^t| < 10^{-0.5} \sim 0.3$ MeV. This expo-
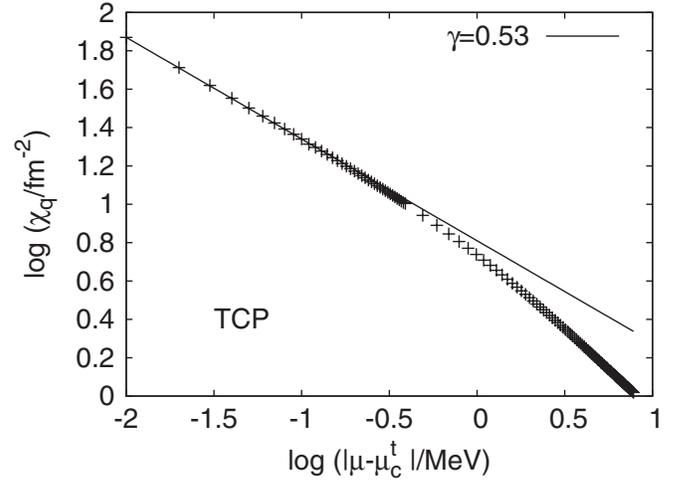
FIG. 16. The logarithm of the quark number susceptibility around the TCP as a function of the logarithm of the chemical potential in the vicinity of the TCP. The solid line is a linear fit.

nent is consistent with mean-field theory which predicts a critical exponent $\gamma_q = 1/2$. This is also expected due to the Gaussian fixed point structure of the TCP.

Leaving the chiral limit, the universality class of the CEP is that of the three-dimensional Ising model. Using again a path parallel to the μ-axis from lower μ towards the CEP we repeat the calculation of the critical exponent. In Fig. 17 χ_q is shown versus the distance from the CEP. It is interesting to see, that there seems to be two different scaling regimes, which we indicated with two linear fit functions in the figure.

The slope for the data points changes between $10^{-0.5}$ MeV $< |\mu - \mu_c^c| < 10^{0.5}$ MeV. We have fitted the data for $|\mu - \mu_c^c| < 10^{-0.5}$ MeV and $> 10^{0.5}$ MeV separately and obtained the critical exponent $\epsilon \sim 0.74$ (solid line) for $|\mu - \mu_c^c| < 10^{-0.5} \sim 0.3$ MeV. For $|\mu - \mu_c^c| > 10^{0.5}$ MeV we also see a linear behavior for several orders
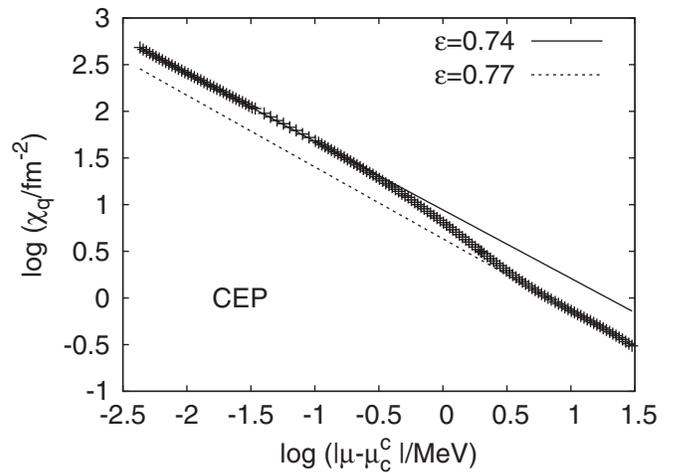
FIG. 17. Same as Fig. 16 for the CEP.

of magnitude. If there is a proper scaling behavior of the susceptibility in this region, the slope would be consistent with an exponent of $\epsilon \sim 0.77$ (dashed line). This change of the exponents could be interpreted as a crossover of different universality classes [38]. One possibility for this crossover phenomenon is that the CEP is somehow affected by the TCP. In Ref. [16] a similar crossover phenomenon between different universality classes in the framework of the CJT potential for QCD in improved-ladder approximation is seen: As they approach the CEP for realistic quark masses ($m_q \sim 5$ MeV), the critical exponent change gradually from those of the tricritical point to those of the 3D Ising model via those of the CEP in the mean-field approximation. In mean-field theory one expects $\epsilon \equiv \gamma/\beta\delta = 2/3$. They find a crossover from the nontrivial critical exponent $\epsilon = 0.57 \pm 0.01$ to the mean-field exponent $\epsilon = 0.68 \pm 0.02$. Contrary to this work, we find a crossover from $\epsilon = 0.77$ to $\epsilon = 0.74$. Thus, at the CEP the susceptibility diverges with the critical exponent $\epsilon \sim 0.74$. This exponent is consistent with the one of the 3D Ising universality class $\epsilon = 0.78$ and is definitely different from the mean-field value $\epsilon = 2/3$. Note also, that the mean-field exponent of a bicritical point (CEP) are in general different from those of a tricritical point. In order to complete the analysis here we summarize the critical exponents of different approaches in Table I.

It is also interesting that the value $|\mu - \mu_c^c| \sim 0.5$ MeV where the slope of the data points changes to a mean-field scaling in Ref. [16] is comparable to our value.

E. The critical region

We are now able to compare the impact of the quantum and thermal fluctuations on the shape of the region around the critical points in the phase diagram. We repeat the calculation of the contour plot of Figs. 6 and 7 in the framework of the RG approach. The result for the scalar susceptibility around the CEP for the same four ratios R_s as in the mean-field approximation is shown in Fig. 18.

As in the mean-field case the region is elongated in the direction of the first-order transition line, but it is now much more compressed. For example, choosing a ratio of $R_s = 15$, the corresponding susceptibility covers an interval from -0.04 to 0.02 in the reduced chemical potential direction and an interval from -0.1 to 0.4 in the temperature direction. In the mean-field case the same ratio covers an interval from -0.8 to 0.1 in the μ direction and from -0.15 to 0.6 in the T direction. While the interval in the

FIG. 18. The contour regions for four different ratios of the scalar susceptibilities $\chi_\sigma(T, \mu)/\chi_\sigma(0, 0)$ ($R_s = 10, 15, 20, 25$) around the CEP in the phase diagram.

temperature direction is comparable in both cases, the effect in the chemical potential direction is dramatic. In the RG calculation the interval is shrunken by almost 1 order of magnitude, despite the fact that the corresponding critical exponents are quite similar!

An similar result is obtained for the critical region of the quark number fluctuations. In order to compare the critical region around the CEP with the one around the TCP we show the quark number susceptibility in Fig. 19 in a larger sector of the phase diagram containing both critical points.

The CEP is far away from the TCP at larger values of the chemical potential and smaller temperature as expected. Because of the sharp transition lines in the chiral limit the critical region around the TCP is chop off in the chirally symmetric phase. Whether there is a robust effect of the TCP on the CEP as stated in Ref. [16] is not seen in this
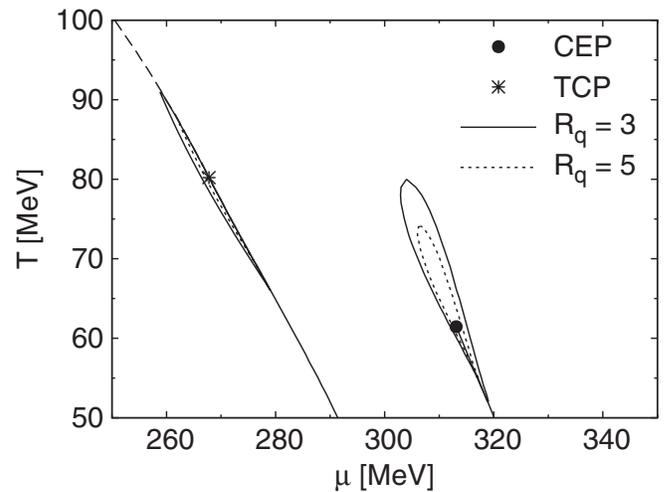
FIG. 19. The contour regions for two different ratios of the quark number susceptibilities $R_q = \chi_q(T, \mu)/\chi_q^{\text{free}}(T, \mu)$ around the CEP and TCP in the phase diagram.

TABLE I. Critical exponents for the 3D Ising model.

	α	β	γ	δ	ν	η	Ref.
mean-field	0	1/2	1	3	1/2	0	[38]
ϵ-exp. (5 loops)	0.11	0.327	1.24	4.80	0.631	0.04	[39]
num. sim.	0.12	0.31	1.25	5.20	0.64	0.06	[40]

work. But this important issue including the quark mass dependence of the susceptibilities is postponed to a further analysis.

V. SUMMARY AND CONCLUSION

Using a Wilsonian renormalization group approach, we have analyzed the phase diagram of hadronic matter in the two-flavor quark-meson model. This model captures essential features of QCD, such as the spontaneous breaking of chiral symmetry in the vacuum and can therefore yield valuable insight into the critical behavior, associated with chiral symmetry. Of special importance is the emergence of a CEP which is intensely discussed at present, in connection with fluctuation signals in heavy-ion collisions. Here the size of the critical region around the CEP is of special importance. Most studies of this issue, available in the literature, have been performed in the mean-field approximation, which neglects thermal and quantum fluctuations. These can be assessed, however, in the RG approach which is able to correctly predict critical exponents in the vicinity of critical points of the phase diagram.

The main results of this work can be summarized as follows:

(1) From universality arguments it is expected that the quark-meson model (and most likely QCD) has a TCP in the chiral limit. For the parameter set chosen in this paper, a mean-field calculation is not able to find such a point, while the RG predicts its existence. The expected critical behavior is also reproduced. Because of the Gaussian fixed-point structure at the TCP mean-field exponents are expected what we could verify.

(2) When effects of finite current quark masses (finite pion masses) are included, a CEP emerges in both the mean-field and the RG calculation. By analyzing the scalar- and quark number susceptibilities we find

that the RG calculation yields nontrivial critical exponents, consistent with the expected 3D Ising universality class. Close to the CEP our exponent is consistent with the Ising class but we also see a novel crossover phenomenon.

(3) As a consequence of fluctuations, the size of the critical region around the CEP is substantially reduced, as compared to mean-field results. This is particularly true in the μ-direction, where a shrinkage by almost 1 order of magnitude is observed. This may have consequences for the experimental localization of the CEP in the phase diagram since it further complicates its detection through event-by-event fluctuations.

The success of the RG approach in predicting the expected critical behavior of the thermodynamics in the quark-meson model encourages us to pursue the issue of the existence of a CEP in the phase diagram of strongly interacting matter and its location in the (T, μ)-plane further. It is known from lattice studies that the strange quark plays a major role. We therefore intend to extend the analysis to three quark flavors [41]. One of the drawbacks of the quark-meson model is the lack of explicit gluonic degrees of freedom, which are known to play a big role in the thermodynamics of QCD and are associated with confinement aspects of the theory. One possibility to incorporate such effects is the coupling of the quark-meson model to Polyakov-loop model [42,43], as put forward in [44]. Work in this direction is in progress [45].

ACKNOWLEDGMENTS

[1] M. A. Stephanov, K. Rajagopal, and E. V. Shuryak, Phys. Rev. D **60**, 114028 (1999).

[2] M. A. Stephanov, Int. J. Mod. Phys. A **20**, 4387 (2005).

[3] S. Datta, F. Karsch, P. Petreczky, and I. Wetzorke, Phys. Rev. D **69**, 094507 (2004).

[4] M. Asakawa and K. Yazaki, Nucl. Phys. **A504**, 668 (1989).

[5] A. Barducci, R. Casalbuoni, S. De Curtis, R. Gatto, and G. Pettini, Phys. Lett. B **231**, 463 (1989).

[6] A. Barducci, R. Casalbuoni, S. De Curtis, R. Gatto, and G. Pettini, Phys. Rev. D **41**, 1610 (1990).

[7] J. Berges and K. Rajagopal, Nucl. Phys. **B538**, 215 (1999).

[8] Z. Fodor and S. D. Katz, Phys. Lett. B **534**, 87 (2002).

[9] P. de Forcrand and O. Philipsen, Nucl. Phys. **B642**, 290 (2002).

[10] C. R. Allton, S. Ejiri, S. J. Hands, O. Kaczmarek, F. Karsch, E. Laermann, and C. Schmidt, Phys. Rev. D **68**, 014507 (2003).

[11] M. A. Stephanov, Prog. Theor. Phys. Suppl. **153**, 139 (2004); Int. J. Mod. Phys. A **20**, 4387 (2005)

[12] R. D. Pisarski and F. Wilczek, Phys. Rev. D **29**, 338 (1984).

[13] A. Barducci, R. Casalbuoni, G. Pettini, and R. Gatto, Phys. Rev. D **49**, 426 (1994).

[14] M. A. Halasz, A. D. Jackson, R. E. Shrock, M. A. Stephanov, and J. J. M. Verbaarschot, Phys. Rev. D **58**, 096007 (1998).

[15] M. Harada and A. Shibata, Phys. Rev. D **59**, 014010 (1998).

[16] Y. Hatta and T. Ikeda, Phys. Rev. D **67**, 014028 (2003).

[17] H. Fujii, Phys. Rev. D **67**, 094018 (2003).

[18] N. Brouzakis and N. Tetradis, Nucl. Phys. **A742**, 144 (2004).

[19] C. Nonaka and M. Asakawa, Phys. Rev. C **71**, 044904 (2005).

[20] B.-J. Schaefer and J. Wambach, Nucl. Phys. **A757**, 479 (2005).

[21] O. Scavenius, A. Mocsy, I. N. Mishustin, and D. H. Rischke, Phys. Rev. C **64**, 045202 (2001).

[22] J. Kapusta, *Finite-Temperature Field Theory* (Cambridge University Press, Cambridge, England, 1989).

[23] In order to compare the resulting expressions directly with the RG treatment to be discussed later we consider derivatives w.r.t. the squared field σ^2, which has numerical advantages.

[24] H. Fujii and M. Ohtani, Phys. Rev. D **70**, 014016 (2004).

[25] F. Karsch, Lect. Notes Phys. **583**, 209 (2002).

[26] T. Hatsuda and T. Kunihiro, Phys. Rep. **247**, 221 (1994).

[27] R. B. Griffiths and J. C. Wheeler, Phys. Rev. A **2**, 1047 (1970).

[28] S.-B. Liao, Phys. Rev. D **53**, 2020 (1996).

[29] B.-J. Schaefer and H.-J. Pirner, Nucl. Phys. **A660**, 439 (1999).

[30] D. F. Litim and J. M. Pawlowski, Phys. Rev. D **66**, 025030 (2002).

[31] D. F. Litim and J. M. Pawlowski, Phys. Lett. B **546**, 279 (2002).

[32] D. F. Litim and J. M. Pawlowski, Phys. Rev. D **65**, 081701 (2002).

[33] D. F. Litim, J. M. Pawlowski, and L. Vergara, hep-th/0602140.

[34] O. Bohr, B.-J. Schaefer, and J. Wambach, Int. J. Mod. Phys. A **16**, 3823 (2001).

[35] F. Karsch, E. Laermann, and A. Peikert, Nucl. Phys. **B605**, 579 (2001).

[36] C. R. Allton, M. Doering, S. Ejiri, S. J. Hands, O. Kaczmarek, F. Karsch, E. Laermann, and K. Redlich, Phys. Rev. D **71**, 054508 (2005).

[37] S. A. Gottlieb, W. Liu, D. Toussaint, R. L. Renken, and R. L. Sugar, Phys. Rev. Lett. **59**, 2247 (1987).

[38] W. Gebhardt and U. Krey, *Phasenübergänge und kritische Phänomene* (Vieweg, Braunschweig, 1980).

[39] J. Zinn-Justin, *Quantum Field Theory and Critical Phenomena* (Oxford University Press, New York, 1999).

[40] R. Guida and J. Zinn-Justin, Nucl. Phys. **B489**, 626 (1997).

[41] B.-J. Schaefer, M. Wagner, and J. Wambach (work in progress).

[42] A. Dumitru, J. Lenaghan, and R. D. Pisarski, Phys. Rev. D **71**, 074004 (2005).

[43] A. Dumitru and R. D. Pisarski, Phys. Rev. D **66**, 096003 (2002).

[44] C. Ratti, M. A. Thaler, and W. Weise, Phys. Rev. D **73**, 014019 (2006).

[45] B.-J. Schaefer, J. M. Pawlowski, and J. Wambach (work in progress).